Optics & Laser Technology 192 (2025) 113447

Contents lists available at ScienceDirect

Optics and Laser Technology

journal homepage: www.elsevier.com/locate/jolt

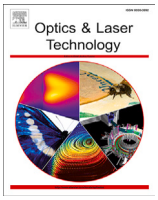

Full length article

Gallium nitride: a strong candidate to replace GaAs as base material for optical photovoltaic converters in space exploration

Javier F. Lozano [a,*], Natalia Seoane [a], J.M. Guedes [a], Enrique Comesaña [b], Julian G. Fernandez [c], Florencia M. Almonacid [d], Eduardo F. Fernández [d], Antonio García-Loureiro [a]

[a] Centro Singular de Investigación en Tecnoloxías de Información (CiTiUS), Departamento de Electrónica e Computación, Universidade de Santiago de Compostela, Rúa de Jenaro de la Fuente, s/n, Santiago de Compostela, 15782, Spain
[b] Escola Politécnica Superior de Enxeñaría, Departamento de Electrónica e Computación, Universidade de Santiago de Compostela, Rúa Benigno Ledo, s/n, Campus Terra, Lugo, 27002, Spain
[c] Escola Técnica Superior de Enxeñaría, Departamento de Electrónica e Computación, Universidade de Santiago de Compostela, Rúa de Lope Gómez de Marzoa, s/n, Campus Vida, Santiago de Compostela, 15705, Spain
[d] Advances in Photovoltaic Technology (AdPVTech), CEACTEMA, University of Jaén, Edificio C-6, Campus de las Lagunillas, Jaén, 23071, Spain

HIGHLIGHTS

- Gallium nitride is proposed as a base material for ultra-high efficiency optical photovoltaic converters due to its high bandgap energy.
- The behavior of GaN-based power converters under several temperatures and changes in the design parameters is discussed.
- The power converters based on GaN obtain a maximum efficiency of 79.6 % at 100 W cm^{-2}, which is more than a 10 % higher than the state-of-the-art.
- GaN based power converters show high resilience to surface recombination and series resistance losses.
- Results support the idea that GaN has the potential to substitute GaAs as a base material for optical photovoltaic converters, especially in harsh environments such as those present on space applications.

ARTICLE INFO

Keywords:
High power laser transmission
Optical photovoltaic converters
Gallium nitride
Wide bandgap
Space exploration

ABSTRACT

High power laser transmission technology is expected to play an important role in spatial exploration. To increase the amount of power delivered, some issues must be addressed. Currently, optical photovoltaic converters are based on GaAs, a material with a bandgap energy of 1.42 eV. In this work we propose gallium nitride (GaN) as base material for optical photovoltaic converters due to its high bandgap (3.39 eV), which reduces both ohmic and intrinsic entropic losses, and its high thermal conductivity and resistance to radiation damage, making it suitable for space applications. We have optimized several GaN optical photovoltaic converter devices under a wide range of laser power densities and temperatures. The resilience to variations in the design parameters is also tested. Results show that, due to their large bandgap energy, GaN devices could suffer from fewer performance losses with the temperature when compared to other materials with lower bandgaps. The devices show great tolerance to variations in the P layer (bottom layer), while the N layer thickness and doping concentration must be carefully manufactured. When compared to GaAs-based devices, GaN shows higher efficiency across the entire laser power density range, achieving efficiencies near 80 % and surpassing the current state-of-the-art power converter by ≈10 % at 10 W cm^{-2}. The proposed GaN devices show a peak of performance at a laser power density as high as 100 W cm^{-2}. Although manufacturing issues could degrade the efficiency of GaN power converters, this results position GaN as a promising material for a new generation of ultra-high efficient optical photovoltaic converters.

* Corresponding author.
Email address: javierfernandez.lozano@usc.es (J.F. Lozano).
URL: https://citius.gal/team/javier-fernandez-lozano (J.F. Lozano).

https://doi.org/10.1016/j.optlastec.2025.113447
Received 4 December 2024; Received in revised form 27 February 2025; Accepted 23 June 2025
Available online 1 July 2025

1. Introduction

High-power laser transmission has emerged as a key technology for far-field wireless power transfer [1]. This method involves using lasers to deliver power to a photovoltaic receiver, which offers distinct advantages such as electrical isolation and the avoidance of electromagnetic interference [2]. Laser transmission can be used through free space, making it ideal for aerospace applications, or via optical fibers, which could replace traditional copper wires, significantly reducing the risk of sparks—an important consideration in ATEX-compliant environments [3]. Applications of this technology range from optically powering aerial vehicles [4] and remote antennas [5], to satellites [6,7] even allowing the simultaneous transfer of power and data [8,9]. Recently, the space applications for this technology have been attracting a lot of attention [10]. In those harsh environments, the degradation and temperature management of the system is a critical point to address for the success of the technology [11].

Current photovoltaic receivers, often referred to as optical photovoltaic converters (OPC), are primarily based on III–V semiconductor materials like GaAs [12]. OPCs have surpassed 60 % conversion efficiency at room temperature [13], with the latest advancements setting a record efficiency of 68.9 % at a power density of 11.4 W cm^{-2}. This is a GaAs-based device, which implemented an optical cavity that minimizes transmission and thermalization losses [14] in the common horizontal optical photovoltaic converter architecture (hOPC). However, as the input power density increases, the efficiency of this device suffers performance losses due to ohmic losses [14]. To address this issue, new architectures have been proposed, such as vertical arrangements [15,16] or multijunctions like the Vertical Epitaxial Hetero-Structure Architecture (VEHSA) [17,18]. The latter consists of monolithically stacked p/n junctions connected by tunnel junctions [13], allowing for higher voltage and reduced current, thereby minimizing Joule heating losses and increasing the output optimal load, mitigating the external resistive losses [18]. These devices have achieved efficiencies of 66.3 % at laser power densities of 150 W cm^{-2}. However, the optimization of VEHSA devices is challenging because of the extreme difficulty in evaluating their individual cell currents [19]. Also, they suffer from current mismatch due to the temperature effects, which reduce the overall efficiency of the device at temperatures different from the one considered in the design of the converter [20,21].

To further improve this technology, the use of high-bandgap materials has been proposed [22–25]. The main benefit of these materials is the higher energy of the incident photons, which increases the output voltage and reduces the current. This not only reduces the series resistance losses, but also increases the output optimal load, allowing the development of high voltage OPCs without the need to rely on multi-junction devices, thus avoiding current-matching vulnerabilities with temperature variations [26]. Besides, the use of high-bandgap materials reduces intrinsic entropic losses, increasing the overall efficiency of the OPCs. Silicon carbide, a semiconductor commonly used in power electronics [27], has recently been suggested as the base material for OPCs [28,29].

Gallium nitride (GaN) is also a very promising candidate. Over the last few decades, this compound and related ternary materials, such as AlGaN and InGaN, have been widely used in optoelectronic components and have recently emerged as key materials in the new generation of power electronic devices [30,31]. Indeed, efforts are being made to manufacture high-quality, low-defect-density GaN crystals [32]. The wurtzite GaN high bandgap (3.39 eV) [33] and high electron mobility [34] make it a sound choice as a base material for optical photovoltaic converters. Furthermore, GaN demonstrates strong resistance to radiation damage, exceptional hardness, and high thermal conductivity [35], along with high chemical stability [36]. These properties are of great interest in harsh environments, such as those encountered in space applications.

Although the properties of GaN are more suitable for OPCs in these environments than those of GaAs, a suitable light source must match the effectiveness of GaN OPCs for this technology to succeed. Currently, monochromatic light sources with high efficiencies are available for the working wavelengths of GaAs-based OPCs. However, this is not the case for GaN-based OPCs, though recent efforts are being made to improve the efficiency of monochromatic light at these wavelengths [37,38].

In this study, we assess the potential of GaN as a base material for OPCs by optimizing multiple GaN-based devices under several laser power densities using the common horizontal optical photovoltaic converter (hOPC) configuration. To evaluate the impact of temperature, a key parameter in aggressive environments to the OPCs or when very high laser power densities are delivered to the converters, we performed these optimizations at several temperature values. Additionally, we tested the resilience of GaN OPCs to variations in the optimized design parameters, anticipating potential challenges in the manufacturing process. Finally, we compare the performance of GaN OPCs with other state-of-the-art devices. Results indicate a promising pathway toward efficiently transmitting high power energy densities using GaN as base material for OPCs.

2. Methodology

This section describes the physical properties of the materials used in this work, as well as the main models employed in the simulation framework. Finally, the device modeling insights and optimization techniques are shown.

2.1. Material properties

Fig. 1 compares GaN and GaAs (the preferred base material in state-of-the-art OPCs) key physical properties that affect OPC performance. The wurtzite GaN bandgap energy is 3.39 eV at room temperature [33], notably higher than that of GaAs (1.42 eV). This difference benefits the GaN, reducing both entropic and series resistance losses. The absorption coefficient of GaN (84×10^3 cm^{-1}) [39] is also higher than that of GaAs (12.3×10^3 cm^{-1}) at the chosen operation wavelengths (356 nm for GaN, 808 nm for GaAs), which allows it to absorb most of the incident beam in thinner OPCs, saving material. The electron and hole mobilities are higher for GaAs (8000/390 cm^2 V^{-1} s^{-1} for e^-/h^+, respectively) than for GaN (2000/170 cm^2 V^{-1} s^{-1} for e^-/h^+, respectively)[40]. Both the thermal conductivity and the melting point are higher for GaN (2.2 W cm^{-1} K^{-1} and 2500 °C) than for GaAs, (0.5 W cm^{-1} K^{-1} and

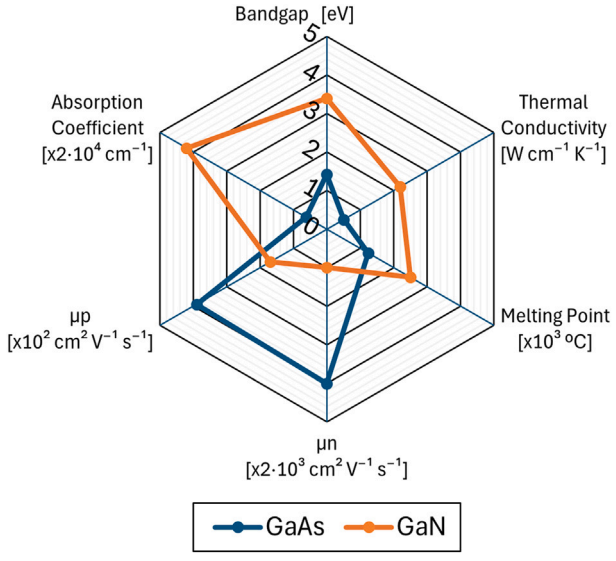

Fig. 1. Relevant material properties in OPC technology for GaN [30,33,41,42] and GaAs.

Table 1
Arora mobility coefficients for electrons and holes [40].

	μ_{min}	μ_{max}	N_{ref}	β_1	β_2	β_3	β_4	ζ
	[$cm^2\ V^{-1}\ s^{-1}$]	[$cm^2\ V^{-1}\ s^{-1}$]	[cm^{-3}]	–	–	–	–	–
e^-	115	1800	7e16	−1.37	−1.37	3.02	0.81	0.8
h^+	12	167	3e17	2.0	−2.34	0.869	−2.311	2.0

1238 °C). This becomes relevant in working environments with extreme conditions, like in space applications. These thermal properties could position GaN as a sounding candidate for applications such as optical powering of rovers on the moon's surface or even deep-space satellites.

2.2. Physical models

This subsection describes the temperature-dependent models used during the simulations. The dependence of low-field mobility with doping and temperature is taken from Sabui et al. [40] where several experimental and modeling studies have been performed. The analytical expression follows the Arora model [43]:

$$\mu_{(n/p)}(T,N) = \mu_{min(n/p)}\left(\frac{T}{300}\right)^{\beta_1} + \frac{\left(\mu_{max(n/p)} - \mu_{min(n/p)}\right)\left(\frac{T}{300}\right)^{\beta_2}}{1 + \left[\frac{N}{N_{ref}\left(\frac{T}{300}\right)^{\beta_3}}\right]^{\zeta\left(\frac{T}{300}\right)^{\beta_4}}} \tag{1}$$

where $\mu_{(n/p)}(T,N)$ is the doping and temperature dependent electron/hole mobility, $\mu_{min(n/p)}$ and $\mu_{max(n/p)}$ the reference mobility parameters for high and low doping values, respectively, N the doping value, N_{ref} a doping reference value, T the lattice temperature and β_1, β_2, β_3, β_4 and ζ are fitting parameters. The coefficients for electrons and holes are presented in Table 1.

The bandgap reduction due to temperature is modeled with the Varshni expression [44]:

$$E_g(T) = E_g(0) - \frac{\alpha_{Eg}\cdot T^2}{T + \beta_{Eg}} \tag{2}$$

where $E_g(T)$ is the temperature-dependent bandgap energy, $E_g(0)$ is the bandgap energy at 0 K and α_{Eg} and β_{Eg} are fitting parameters. The coefficients for GaN are $\alpha_{Eg} = 9.09\cdot 10^{-4}$ eV K^{-1} and $\beta_{Eg} = 830$ K [40].

Regarding the bandgap narrowing (BGN) due to carrier concentration, in n-type GaN, this effect is modeled according to the Jain–Roulston model [40]:

$$\Delta E_g(T) = Z\cdot n^{\frac{1}{3}} \tag{3}$$

where Z is a fitting parameter with value 1.15×10^{-8} eV [40] and n is the electron density.

Due to the high bandgap of GaN, a good characterization of the incomplete ionization is required. The concentration of ionized dopants is modeled as:

$$N_D^+ = \frac{N_D}{1 + g_B\frac{n}{N_C}exp\left(\frac{\Delta E_D}{K_B T}\right)} \tag{4}$$

$$N_A^+ = \frac{N_A}{1 + g_B\frac{p}{N_V}exp\left(\frac{\Delta E_A}{K_B T}\right)} \tag{5}$$

where the degeneracy of the electronic state, g_B, has a value of 2 for GaN. N_D and N_A are the total donor and acceptor doping concentrations, p the hole concentration and N_C and N_V are the effective density of states in the conduction and valence bands, respectively. The donor and acceptor activation energies (ΔE_D and ΔE_A, respectively) are effectively reduced by the high carrier concentration in semiconductors which is also incorporated in the incomplete ionization model. The dependence of $\Delta E_{D/A}$ on the carrier concentration (here using N_D^+/N_A^- as carrier concentration for electrons and holes, in each case) is modeled according to:

$$\Delta E_{D/A} = E_{D/A,0} - \alpha_{(n/p)}\cdot\left(\frac{N_D^+}{N_A^-}\right)^{1/3} \tag{6}$$

where $\Delta E_{D/A,0}$ are the donor and acceptor ionization energies at very low doping levels, with values of 17 me V and 240 me V respectively, and $\alpha_{(n/p)}$ are fitting parameters, with values 3.4×10^{-9} and 3.14×10^{-8} eV cm [40].

The main recombination mechanisms are included in the simulation framework, these being the optical or band-to-band recombination, Shockley–Read–Hall (SRH) or trap-assisted recombination, Auger recombination and surface recombination. The parameters for these models are taken from experimental data [34,36,45,46]. The band to band recombination is modeled as:

$$R_{np}^{OPT} = C_c^{OPT}(np - n_i^2) \tag{7}$$

being n and p the electron and hole concentrations, n_i the intrinsic carrier concentration and C_c^{OPT} the optical experimental coefficient for a material. The SRH recombination can be expressed as:

$$R_{net}^{SRH} = \frac{np - n_i^2}{\tau_p\left(n + n_i exp\frac{E_{trap}}{k_B T}\right) + \tau_n\left(p + n_i exp\frac{-E_{trap}}{k_B T}\right)}, \tag{8}$$

where:

$$\tau_{n,p} = \frac{\tau_0}{1 + \left(\frac{N}{N_{norm}}\right)^{\gamma}}, \tag{9}$$

being E_{trap} the difference between the trap energy level and the intrinsic Fermi level, k_B the Boltzmann constant, $\tau_{n,p}$ the effective electrons and holes lifetimes, τ_0 the longest lifetime observed in undoped crystal, N the total doping concentration, N_{norm} a doping concentration which operates as a normalization constant and γ a fitting parameter.

Auger recombination is modeled as follows:

$$R_{AUGER} = C_n(pn^2 - nn_i^2) + C_p(np^2 - pn_i^2), \tag{10}$$

where C_n and C_p are the experimental Auger coefficients for a given material. All the relevant recombination parameters are summarized in Table 2. In addition, we considered the highest surface recombination (SR) velocity reported in the literature (worst case scenario, 7.5×10^4 cm s^{-1}) [46]. Note that the SR follows a decreasing trend when increasing the bandgap energy [46]. In this sense, GaN-based hOPCs would benefit from the high bandgap energy.

Table 2
Relevant recombination parameters used in the course of the simulations.

Recombination model	Parameter		Units	References
SRH	τ_0^n $12\cdot 10^{-9}$	τ_0^p $12\cdot 10^{-9}$	[s]	[34]
Auger	C_n $2.6\cdot 10^{-31}$	C_p $2.6\cdot 10^{-31}$	[cm^{-6}]	[45,47]
Optical	C_c^{OPT} $2.4\cdot 10^{-11}$		[cm^{-6}]	[36,48]

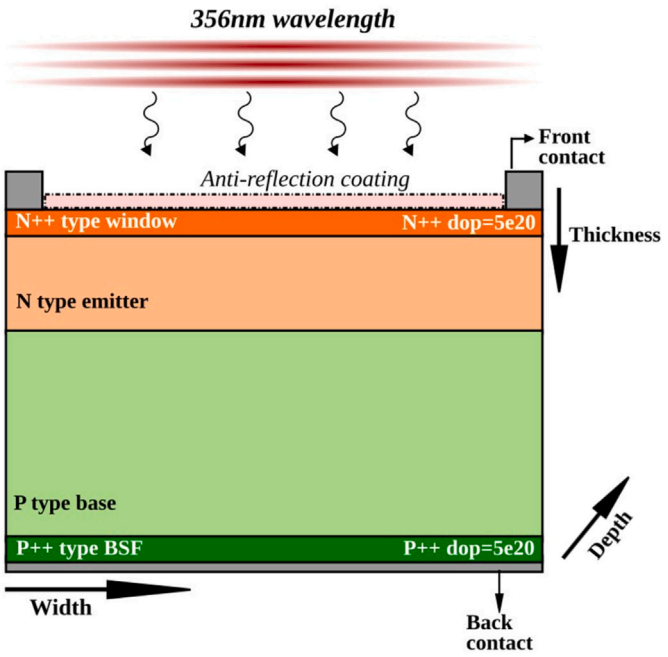

Fig. 2. GaN horizontal optical photovoltaic converter (hOPC) structure.

2.3. Device modeling and optimization

We investigate the feasibility of GaN as base material for OPCs through the conventional horizontal optical photovoltaic converter (hOPC) architecture, see a scheme in Fig. 2. The structure consists of four layers with N+/N/P/P+ doping types. Since the generation and transport processes occur in the vertical direction, the width of the devices is set to 10 μm to save computational costs. The third dimension (depth) is also set to 1 μm^2 to save computational costs, since it does not affect the obtained results. We emulate the behavior of an anti-reflective coating by setting total transmittance in the illumination area, which is a realistic approximation because the device is illuminated with only one wavelength. The cathode is placed at the top of the device, covering a 3 % of the illumination area, while the anode is placed along the bottom of the device. Since these modeled devices are very small (with an illumination area of 10 μm^2), the output current is very low and the effect of the ohmic losses is negligible. To account for this effect in a realistic way we scaled the resistivity of the contacts proportionally to the difference with an experimental OPC's area, specifically to a 10x10 mm^2, as in Shan et al. [49], so the ohmic losses of the modeled OPC are comparable to those of the experimental device.

In this work we have employed Silvaco Atlas [50], which is a widely used TCAD simulator for modeling all kinds of semiconductor devices, including photovoltaic devices. It has been previously applied to model optical photovoltaic converters [15], multijunction concentrator solar cells [51] and VEHSA devices [17]. The J-V characteristics of the devices are obtained by solving the Poisson and charge continuity equations. The optimization of the hOPC devices was performed with an in-house-built multivariable iterative process [28], varying the design parameters in discrete steps to find the optimum design that maximizes the efficiency. These parameters are the thicknesses and doping values of the N and P layers.

3. Results

This section shows the optimization results for GaN hOPCs under several laser power densities and temperatures ranging from 200 to 700 K. First, the optimum design parameters and conversion efficiencies are shown, as well as the JV curves at several temperatures. After that, the resilience of the optimum devices to changes in the design parameters is tested by sweeping the layer thicknesses and doping values. Finally, a comparison of the optimum GaN hOPCs at room temperature with other state-of-the-art devices is presented.

3.1. Device design parameters and optimization results

The GaN hOPC design parameters are optimized for a wide range of laser power densities (1, 10, 100 and 1000 W cm^{-2}) and temperatures (200, 300, 400, 500, 600 and 700 K). Fig. 3 shows the optimum N and P layer thicknesses for the laser power density and temperature ranges studied. The optimum N layer thickness is in the range of 0.04–0.20 μm and consistently increases with lower temperatures and higher laser power density values. However, sweeping the N layer thickness within the optimum range in any of those devices results in efficiency differences no larger than ≈1 %. The P layer thickness optimum values are in the range of 0.40–0.75 μm, being 0.50/0.55 μm the optimum values for all devices except for the hOPC optimized at 200 K and 1000 W cm^{-2} which requires a P layer thickness of 0.75 μm. However, this device only losses a 0.3 % efficiency conversion when the P layer thickness is set to 0.50 μm.

The optimum doping concentrations for the N and P layers are shown in Fig. 4. In the N layer, the optimum N doping values increase with temperature, from 1×10^{17} cm^{-3} at 200 K to 1×10^{18} cm^{-3} at 700 K, with no dependence on the laser power density. In the P layer, all the devices show optimum doping values in the range of 5×10^{17}–1×10^{18} cm^{-3}, except for the device optimized at 200 K and 1000 W cm^{-2}, whose P layer optimum doping value is 5×10^{19} cm^{-3}. The effect of varying the design parameters of the proposed devices will be carefully studied in Section 3.2.

The efficiencies of the optimized devices vs. The laser power density at several temperatures are shown in Fig. 5. Note that the GaN hOPCs

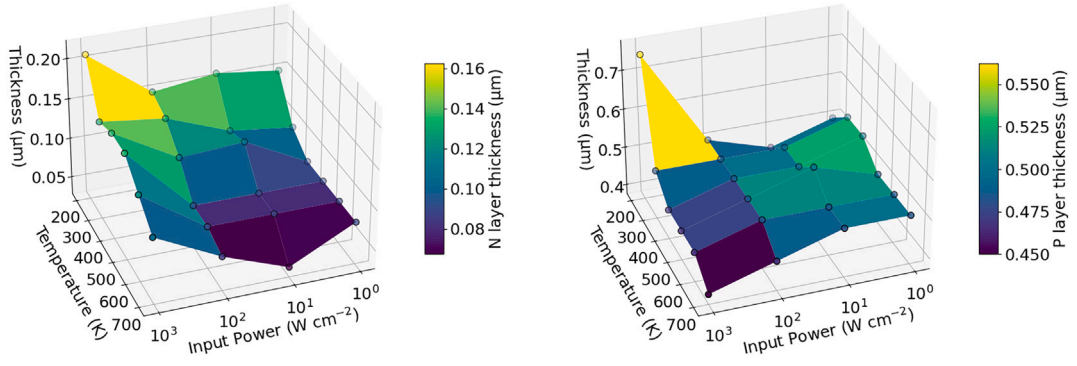

Fig. 3. Optimum thicknesses of the N layer (left) and P layer (right) for the laser power density range [1–1000 W cm^{-2}] and the temperature range [200–700 K].

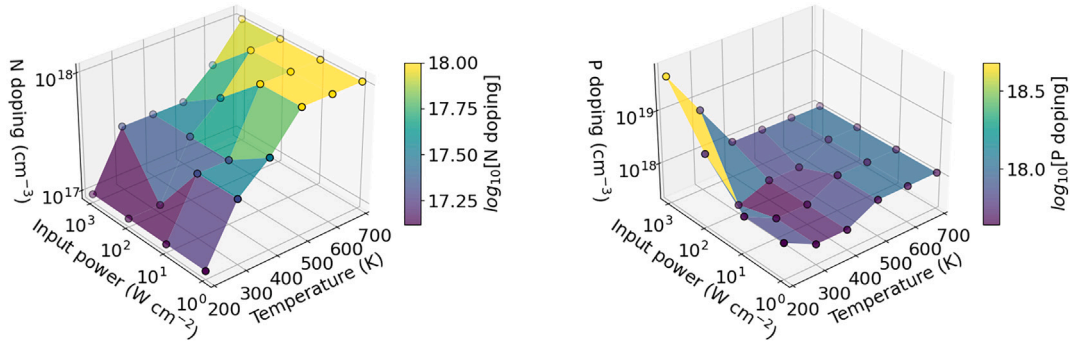

Fig. 4. Optimum doping values of the N layer (left) and P layer (right) for the laser power density range [1–1000 W cm^{-2}] and the temperature range [200–700 K].

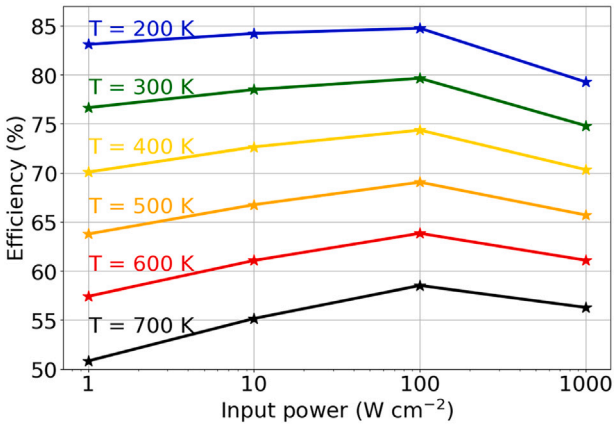

Fig. 5. Efficiency versus the input power density for temperatures ranging from 200 to 700 K.

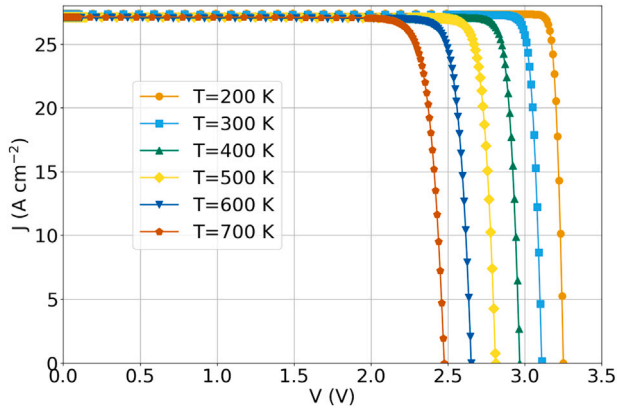

Fig. 6. JV curves for the devices optimized at 100 W cm^{-2} for temperatures ranging from 200 to 700 K.

consistently increase the efficiency with the laser power density until 100 W cm^{-2}, at all studied temperatures, from which point the series resistance losses degrade the conversion efficiency. An increase in temperature produces more intrinsic carrier concentration, which reduces the V_{OC} (and thus the efficiency) as seen in Eq. (11):

$$V_{oc} = \frac{K_B T}{q} ln\left[\frac{(N + \Delta n)\,\Delta n}{n_i^2}\right] \tag{11}$$

where $K_B T/q$ is the thermal voltage, N is the doping concentration, Δn is the excess carrier concentration and n_i is the intrinsic carrier concentration. Indeed, at 1 W cm^{-2}, the efficiency decreases from 83.1 % at 200 K to a 50.8 % at 700 K, a consistent ≈6.5 % reduction each 100 K (see Fig. 5). As the laser power density increases, the reduction in efficiency due to temperature becomes less pronounced, decreasing by roughly 5.2 % for every 100 K at 100 W cm^{-2}.

Fig. 6 shows the JV curves of these devices at 100 W cm^{-2} for all the analyzed temperatures. Note that the short circuit current density (J_{SC}) is approximately the same for all devices, with differences no larger than ≈1 % from 200 to 700 K. The V_{OC} values range from 3.25 to 2.48 V for temperatures between 200 and 700 K, which implies an average V_{OC} reduction of ≈ 1.5 mV K^{-1}. For comparison, the average silicon solar cell losses ≈ 2.2 mV K^{-1} [52], and for GaAs solar cells the reduction is around 2.15 mV K^{-1} [53]. Note that the GaN devices benefit from larger bandgap energy, which effectively reduces the V_{OC} losses with temperature [52].

3.2. Resilience to design parameter variation

In this section, we evaluate the resilience of the GaN hOPC to N and P layer doping and thickness variations, analyzing their effect on the main figures of merit (FoMs) of the device, i.e., efficiency, fill factor (FF), open-circuit voltage (V_{OC}) and short-circuit current density (J_{SC}). This study was conducted at room temperature and an input power density of 100 W cm^{-2}. Under these conditions, the optimized GaN hOPC achieves an efficiency of 79.64 % (see Fig. 5). This value was obtained at N/P layer thicknesses of 0.14/0.5 μm and N/P layer doping levels of $1 \times 10^{17}/3 \times 10^{17}$ cm^{-3}, respectively. For each parameter variation, all other variables remain fixed at the values corresponding to the optimal device configuration.

Fig. 7 shows the effect of the N layer doping variations on the hOPC FoMs. For N layer doping values ranging from $1{\times}10^{12}$ to $1{\times}10^{17}$ cm^{-3}, the analyzed FoMs remain practically constant, with efficiency values close to 80 %. However, when the doping is increased beyond 1×10^{17} cm^{-3}, the effect of SRH recombination becomes noticeable, significantly degrading performance. An 18 % efficiency drop is observed at an N layer doping of 1×10^{20} cm^{-3}, compared to the optimum efficiency value. To further explain this behavior, Fig. 8 shows the SRH recombination rates obtained at doping levels of $1{\times}10^{17}$ and $1{\times}10^{20}$ cm^{-3} and the corresponding photogeneration rate along the N layer thickness. The SRH rate at an N doping of 1×10^{20} cm^{-3} can be up to four orders of magnitude higher than the respective value at 1×10^{17} cm^{-3}. Note that in both cases, the photogeneration does not change. This increase in SRH rate also causes a reduction in J_{SC}, lowering its value to as much as 6 A cm^{-2} when N doping reaches 1×10^{20} cm^{-3}. On the other hand, V_{OC} is expected to increase with higher doping levels due to its logarithmic dependence (see Eq. 11), but V_{OC} remains close to 3.10 V across the entire range of doping values analyzed because the high SRH recombination rates mitigate the expected doping-dependent increase.

Fig. 9 shows the impact of the N layer thickness variations on the hOPC FoMs. For the N layer thickness values below 0.3 μm, all the

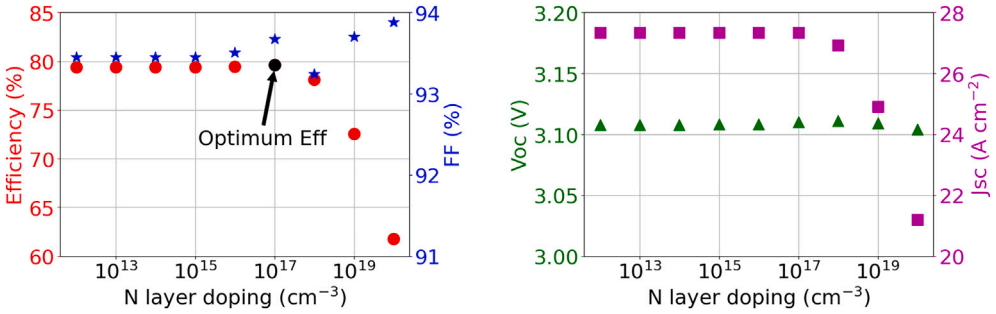

Fig. 7. Variation of efficiency (circles), fill factor (stars), open circuit voltage (triangles) and short circuit current density (squares) versus the doping of the N layer at 100 W cm^{-2} and 300 K. The maximum efficiency value is also indicated.

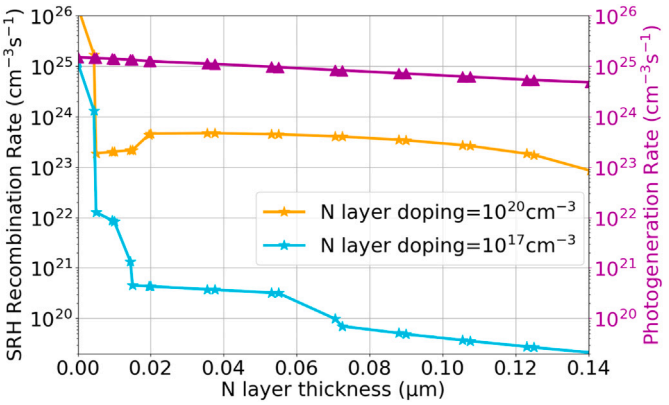

Fig. 8. Variation of photogeneration rate (triangles) and SRH recombination (stars) at two doping levels along the N layer thickness.

studied FoMs remain unchanged, with efficiency values near the optimum. Over that thickness value, efficiency rapidly decreases, dropping to around 45 % at 2 μm. This 34 % loss is due to the recombination of the photogenerated carriers in that layer. For the same reason, J_{SC} decreases to up to 10 A cm^{-2} in the same range. On the other hand, V_{OC} and FF slightly decrease across the entire range, taking values around 3.10 V and between 89 % and 94 %, respectively.

Figs. 10 and 11 show the influence of variations in P layer doping and thickness on the FoMs of the device. This layer demonstrates greater resilience to these parameter variations compared to the N layer. For the P layer doping, efficiency values vary between 77 % and an optimum of 79.64 % for all analyzed doping levels, which is a variation 7 times smaller than that observed in the N layer. J_{SC} does not change until the optimal doping value of 3×10^{17} cm^{-3}, slightly decreasing for larger doping levels. Note that, at a P layer doping of 1×10^{20} cm^{-3}, the J_{SC} only reduces by 1 A cm^{-2}, a value 6 times smaller than the reduction observed when analyzing the same effect in the N layer. This occurs because most carriers are photogenerated in the N layer, leaving fewer carriers in the P layer, observing a SRH recombination rate an order of magnitude lower than that in the N layer. V_{OC} remains constant for doping levels $\leq 3 \times 10^{17}$ cm^{-3} and then increases due to its logarithmic dependence on the doping. This increase appears because the SRH recombination rate does not counterbalance the doping-dependent increase, contrary to what happens in the P layer. FF values are between 91 % and 94 % throughout the entire doping range studied. Meanwhile, any P layer thickness variation between 0.2 μm and 2.0 μm, only changes efficiency by around 1 % at the most. Regarding the J_{SC}, it moderately increases up to 27.5 A cm^{-2} at a thickness of 0.5 μm and then remains constant for larger thickness values. V_{OC} takes values around 3.10 V throughout the range.

Thus, the P layer of the device demonstrates resilience to variations in both doping concentration and thickness, consistently yielding high-performance devices. In contrast, the N layer imposes some limitations on achieving high efficiency. This is because most carrier generation and recombination processes occur within the N layer, where the majority of incident photons are absorbed within the first few tenths of micron. Consequently, when designing a GaN hOPC, the N layer must be carefully tailored.

3.3. Comparative with state-of-the-art

Fig. 12 shows the efficiency vs. The laser power density for the optimum GaN hOPCs at room temperature presented in this work and several state-of-the-art devices, based on GaAs or AlGaAs/GaAs, which represent the current leading technology. To validate our methodology, we modeled a GaAs hOPC (see GaAs hOPC in Fig. 12) based on the experimental device developed by Shan et al. [49] (see Shan 2016 in the Figure), perfectly matching the JV characteristics and the main FoMs

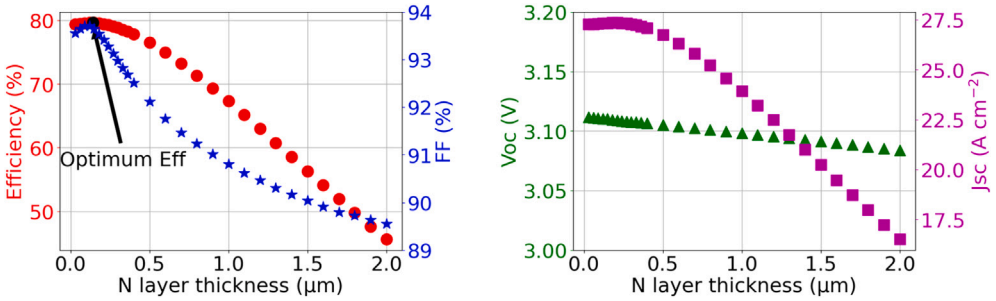

Fig. 9. Variation of efficiency (circles), fill factor (stars), open circuit voltage (triangles) and short circuit current density (squares) versus the thickness of the N layer at 100 W cm^{-2} and 300 K. The maximum efficiency value is also indicated.

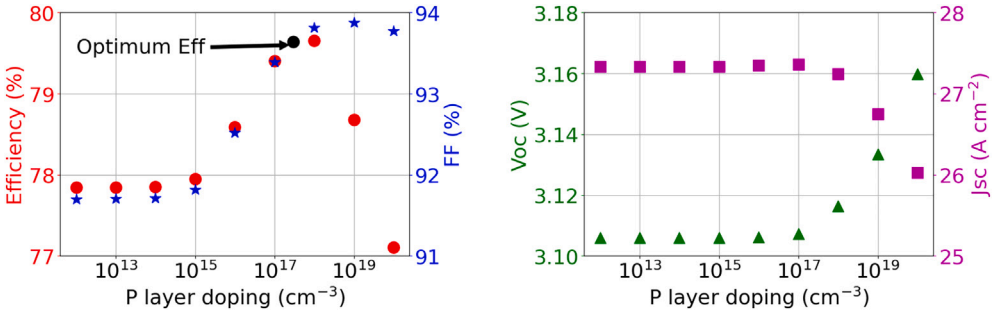

Fig. 10. Variation of efficiency (circles), fill factor (stars), open circuit voltage (triangles) and short circuit current density (squares) versus the doping of the P layer at 100 W cm^{-2} and 300 K. The maximum efficiency value is also indicated.

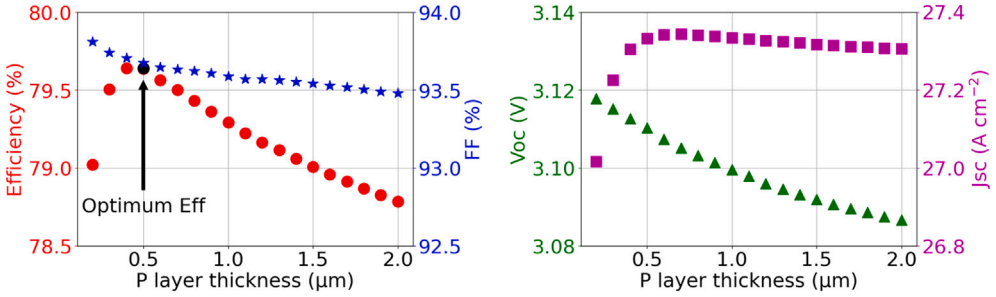

Fig. 11. Variation of efficiency (circles), fill factor (stars), open circuit voltage (triangles) and short circuit current density (squares) versus the thickness of the P layer at 100 W cm^{-2} and 300 K. The maximum efficiency value is also indicated.

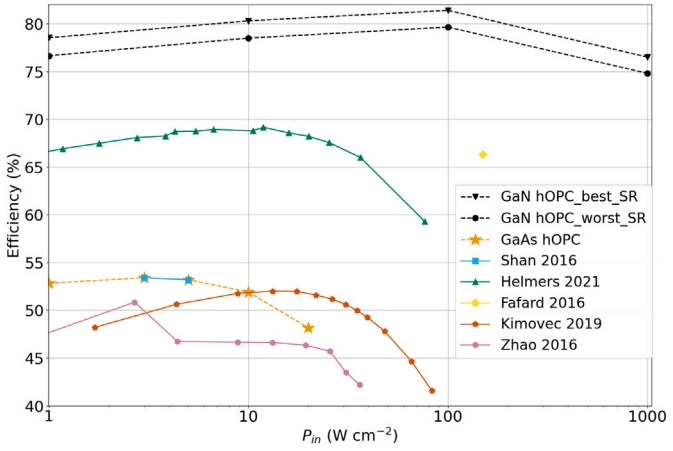

Fig. 12. Comparison of efficiency vs. laser power density (P_{in}) at room temperature for the presented GaN hOPCs, the calibrated GaAs hOPC and state-of-the-art OPCs.

[54] for two P_{in} values (3 and 5 W cm^{-2}). We chose this experimental hOPC due to the amount of detail on the design parameters provided by the authors. Once validated, we extended the laser power density range of this device to higher P_{in} values to fully appreciate the effect of the series resistance losses at larger laser power densities. We also include the GaN optimizations with the lowest SR velocity reported in the literature (5.0×10^3 cm/s). Note that the differences between the best and worst case (7.5×10^4 cm s^{-1}) scenarios are around 2 %, so this effect is not expected to be a limiting factor for the success of this technology.

The current state-of-the-art is a GaAs OPC from Helmers et al. [14] that has demonstrated an impressive efficiency of 68.9 % at 11.4 W cm^{-2} by integrating an optical cavity designed to minimize both transmission and thermalization losses. This is the highest efficiency recorded for an experimental OPC. However, the efficiency of their horizontal OPC declines at higher irradiances due to ohmic losses, dropping to 59.3 % at 76.6 W cm^{-2}. To enable higher power transfer, alternative horizontal designs like the VEHSA architecture, introduced by Fafard et al. [13], employ a strategy of stacking multiple thin photovoltaic semiconductor subcells, which divides the current and reduces series resistance losses. This approach resulted in an efficiency of 66.3 % at 150 W cm^{-2}.

Our proposed GaN hOPC devices exhibit impressive efficiency within the range of 1–100 W cm^{-2}, a typical operating range for OPCs. Optimized at 10 W cm^{-2}, this hOPC reaches an efficiency of 78.5 %, surpassing the record set by Helmers et al. [14] by 9.6 %. The efficiency of the GaN hOPC further increases to 79.64 % at 100 W cm^{-2}. As with other horizontal OPCs, its efficiency decreases at higher laser power densities, mainly due to increasing series resistance losses and Auger recombination. However, across the entire P_{in} range analyzed, the efficiency remains higher than other leading horizontal OPCs, with a relatively mild reduction in efficiency—4.8 % between 100 and 1000 W cm^{-2}. Note that the methodology used for the GaN hOPC is the same as in the Shan validation (GaAs hOPC in Fig. 12), and the GaN device achieves an efficiency conversion 23.8 % higher than the GaAs power converter at 1 W cm^{-2}, while also experiencing less series resistance losses as the P_{in} increases. These differences can only be related to the higher bandgap energy and more suitable material properties of the GaN.

While real GaN hOPC devices are likely to exhibit lower performance due to manufacturing-related losses, such as shunt losses and sheet resistance. However, these results offer a promising outlook for further research into highly efficient OPCs based on GaN, highlighting the best design parameters for each application case.

4. Conclusions

High-power laser transmission technology is currently a highly-relevant topic in space applications. The state-of-the-art for

the photovoltaic receivers or optical photovoltaic converters (OPCs) relies on gallium arsenide (GaAs), a low-bandgap material that limits power transfer due to increased ohmic losses, which degrade efficiency as laser power density increases. Moreover, effective temperature management and resistance to harsh environments are critical to ensure the success of this technology.

In this work we proposed gallium nitride (GaN), a high bandgap compound, as base material for OPCs. This material presents higher thermal conductivity and a greater melting point than GaAs, and also high resistance to radiation. We implemented the standard horizontal optical photovoltaic converter (hOPC) architecture using this semiconductor. The simulation framework included detailed temperature-dependent models. We optimized the GaN-based hOPCs under a wide range of laser power densities (1–1000 W cm^{-2}) and temperatures (200–700 K). Results show consistent efficiency losses when increasing the temperature. However, these losses, which are mainly due to the V_{OC} reduction with the temperature, are lower than for other semiconductors, since the high bandgap of GaN mitigates them. To evaluate the resilience of the optimized OPCs to variations in the design parameters, we performed simulations sweeping the thickness and doping values of the N and P layers, starting from the optimal designs. The N layer (top layer) imposes limitations due to its higher carrier generation, and thus it must be carefully designed. The P layer, on the contrary, performs considerably well for a wide range of layer thicknesses and doping values. To validate our methodology, we also modeled a GaAs hOPC based on an experimental device. The GaN device surpasses this GaAs power converter by 23.8 % at 1 W cm^{-2} and shows lower series resistance losses as power input increases. These performance improvements can be attributed to the GaN higher bandgap energy and its more advantageous material properties, which make it better suited for high-power density operations.

Finally, we presented a comparison with the state-of-the-art and other high-performance devices. Our GaN hOPC devices demonstrate remarkable efficiency across a wide input power operational range of 1–100 W cm^{-2}, a typical range for OPCs, achieving a 78.5 % efficiency at an optimized power density of 10 W cm^{-2} and surpassing the current state-of-the-art device by 9.6 %. As the laser power density increases to 100 W cm^{-2}, the efficiency continues to rise up to 79.64 %. This is 13.34 % higher than the best-performing experimental VEHSA device, which achieves a 66.3 % at 150 W cm^{-2} and requires a more laborious manufacturing process than a single hOPC cell. Like other hOPCs, the efficiency of the GaN devices begins to drop at higher laser power densities due to factors like series resistance losses and Auger recombination. However, even with these challenges, the GaN hOPC maintains superior efficiency compared to other leading hOPCs and experiences these efficiency losses at higher power densities than the GaAs devices, with only a 4.8 % decrease in efficiency between 100 and 1000 W cm^{-2}.

Although the performance of experimental GaN hOPCs is expected to show lower efficiency than the modeled ones due to manufacturing issues, the presented results position GaN as a promising candidate to replace GaAs as base material for power converters, especially in challenging conditions such as those present in space applications.

CRediT authorship contribution statement

Javier F. Lozano: Conceptualization, Data curation, Writing – original draft, Investigation. **Natalia Seoane:** Conceptualization, Funding acquisition, Supervision, Writing – review & editing. **J.M. Guedes:** Data curation, Writing – review & editing. **Enrique Comesaña:** Methodology, Software, Writing – review & editing. **Julian G. Fernandez:** Software, Writing – review & editing. **Florencia M. Almonacid:** Investigation. **Eduardo F. Fernández:** Methodology. **Antonio García-Loureiro:** Conceptualization, Funding acquisition, Project administration, Writing – review & editing.

Declaration of competing interest

The authors declare that they have no known competing financial interests or personal relationships that could have appeared to influence the work reported in this paper.

Acknowledgements

This work has received financial support from the Agencia Estatal de Investigación (Spain) (MCIN/AEI/10.13039/501100011033 code PID2022-141623NB-I00 and PID2022-142709OB-C21/PID2022-142709OA-C22), the Xunta de Galicia - Consellería de Cultura, Educación, Formación Profesional e Universidades (Centro de investigación de Galicia accreditation 2024–2027 ED431G-2023/04 and Reference Competitive Group accreditation ED431C-2022/016) and the European Union (European Regional Development Fund - ERDF/EU). The work of Florencia Almonacid and Eduardo F. Fernández is part of the project PowerForEath (PID2023-147898OB-I00) funded by MICIU/AEI /10.13039/501100011033/ and by ERDF A way of making Europe. This work was supported by a project selected via the Open Space Innovation Platform (https://ideas.esa.int) as a Co-Sponsored Research Agreement and carried out under the Discovery programme of, and funded by, the European Space Agency (contract number: 4000143581).

Data availability

Data will be made available on request.

References

[1] K. Jin, W. Zhou, Wireless laser power transmission: a review of recent progress, IEEE Trans. Power Electron. 34 (4) (2019) 3842–3859.
[2] D. Krut, R. Sudharsanan, W. Nishikawa, T. Isshiki, J. Ermer, N.H. Karam, Monolithic multi-cell GaAs laser power converter with very high current density, in: Conference Record of the IEEE Photovoltaic Specialists Conference, 2002, pp. 908–911.
[3] C. Algora, I. García, M. Delgado, R. Peña, C. Vázquez, M. Hinojosa, I. Rey-Stolle, Beaming power: photovoltaic laser power converters for power-by-light, Joule 6 (2) (2021) 1–29.
[4] N. Kawashima, K. Takeda, H. Matsuoka, Y. Fujii, M. Yamamoto, Laser energy transmission for a wireless energy supply to robots, in: 22nd International Symposium on Automation and Robotics in Construction, ISARC 2005, International Association for Automation and Robotics in Construction (IAARC), 2005, https://doi.org/10.22260/ISARC2005/0068.
[5] C. Vázquez, J.D. López-Cardona, P.C. Lallana, D.S. Montero, F.M.A. Al-Zubaidi, S. Pérez-Prieto, I.P. Garcilópez, Multicore fiber scenarios supporting power over fiber in radio over fiber systems, IEEE Access 7 (2019) 158409–158418.
[6] D. Shi, L. Zhang, H. Ma, Z. Wang, Y. Wang, Z. Cui, Research on wireless power transmission system between satellites, in: 2016 IEEE Wireless Power Transfer Conference, WPTC 2016, vol. 3, IEEE, 2016, pp. 1–4, https://doi.org/10.1109/WPT.2016.7498851.
[7] M. Sanders, J.S. Kang, Utilization of polychromatic laser system for satellite power beaming, in: IEEE Aerospace Conference Proceedings, 2020, pp. 1–7.
[8] M. Matsuura, H. Nomoto, H. Mamiya, T. Higuchi, D. Masson, S. Fafard, Over 40-W electric power and optical data transmission using an optical fiber, IEEE Trans. Power Electron. 36 (4) (2021) 4532–4539.
[9] H. Helmers, C. Armbruster, M.V. Ravenstein, D. Derix, C. Schoner, 6-W optical power link with integrated optical data transmission, IEEE Trans. Power Electron. 35 (8) (2020) 7904–7909.
[10] P. Jaffe, T. Nugent, B. Strassner II, M. Szazynski, Power Beaming, World Scientific, 2024, https://doi.org/10.1142/12438.
[11] E.J. Brandon, R. Bugga, J. Grandidier, J.L. Hall, J.A. Schwartz, S. Limaye, Power beaming for long life venus surface missions, NIAC Phase I Final Report, 2020.
[12] J. Schubert, E. Oliva, F. Dimroth, W. Guter, R. Loeckenhoff, A.W. Bett, High-voltage GaAs photovoltaic laser power converters, IEEE Trans. Electron Devices 56 (2) (2009) 170–175.
[13] S. Fafard, F. Proulx, M.C.A. York, L.S. Richard, P.O. Provost, R. Arès, V. Aimez, D.P. Masson, High-photovoltage GaAs vertical epitaxial monolithic heterostructures with 20 thin p/n junctions and a conversion efficiency of 60 %, Appl. Phys. Lett. 109 (13) (2016) 131107.
[14] H. Helmers, E. Lopez, O. Höhn, D. Lackner, J. Schön, M. Schauerte, M. Schachtner, F. Dimroth, A.W. Bett, 68.9 photonic power conversion enabled by photon recycling and optical resonance, Phys. Status Solidi (RRL)–Rapid Res. Lett. 15 (7) (2021) 1–7.
[15] C. Outes, E.F. Fernandez, N. Seoane, F. Almonacid, A.J. Garcia-Loureiro, GaAs vertical-tunnel-junction converter for ultra-high laser power transfer, IEEE Electron Device Lett. 42 (12) (2021) 1882–1885.
[16] N. Seoane, E.F. Fernández, F. Almonacid, A. García-Loureiro, Ultra-efficient intrinsic-vertical-tunnel-junction structures for next-generation concentrator solar cells, progress in photovoltaics, Res. Appl. 29 (2) (2021) 231–237.
[17] M.C. York, A. Mailhot, A. Boucherif, R. Arès, V. Aimez, S. Fafard, Challenges and strategies for implementing the vertical epitaxial heterostructure architechture

(VEHSA) design for concentrated photovoltaic applications, Sol. Energy Mater. Sol. Cells 181 (2018) 46–52.
[18] S. Fafard, D.P. Masson, Perspective on photovoltaic optical power converters, J. Appl. Phys. 130 (16) (2021) 160901.
[19] J.F. Lozano, N. Seoane, E. Comesaña, F.M. Almonacid, E.F. Fernández, A. García-Loureiro, Photogeneration and performance optimization (PhPO): a new algorithm to improve the performance of vertical epitaxial hetero-structure architecture laser power converters, IEEE Access 11 (2023) 84371–84378.
[20] S.K. Reichmuth, H. Helmers, S.P. Philipps, M. Schachtner, G. Siefer, A.W. Bett, On the temperature dependence of dual-junction laser power converters, Prog. Photovolt. Res. Appl. 25 (1) (2017) 67–75.
[21] F.A. Valera-Albacete, P.M. Rodrigo, E.F. Fernández, The potential of a hybrid optical photovoltaic converter–thermoelectric receiver to enhance conversion efficiency, IEEE Electron Device Lett. 44 (8) (2023) 1360–1363.
[22] E.F. Fernández, A. García-Loureiro, N. Seoane, F. Almonacid, Band-gap material selection for remote high-power laser transmission, Sol. Energy Mater. Sol. Cells 235 (2022) 111483.
[23] E. Oliva, F. Dimroth, A.W. Bett, GaAs converters for high power densities of laser illumination, progress in Photovoltaics, Res. Appl. 16 (4) (2008) 289–295.
[24] M. Lin, W.E. Sha, W. Zhong, D. Xu, Intrinsic losses in photovoltaic laser power converters, Appl. Phys. Lett. 118 (10) (2021) 1–5.
[25] P. Sanmartín, E.F. Fernández, A. García-Loureiro, J. Montes-Romero, A. Cano, P. Martín, I. Rey-Stolle, I. García, F. Almonacid, Design and characterization of a 53.5% efficient gallium indium phosphide-based optical photovoltaic converter under 637 nm laser irradiation at 10 W cm^{-2}, Solar RRL 8 (15) (2024) 2400278.
[26] P. Sanmartín, F. Almonacid, M.A. Ceballos, A. García-Loureiro, E.F. Fernández, Wide-bandgap III–V materials for high efficiency air and underwater optical photovoltaic power transmission, Sol. Energy Mater. Sol. Cells 266 (2024) 112662.
[27] X. She, A.Q. Huang, O. Lucia, B. Ozpineci, Review of silicon carbide power devices and their applications, IEEE Trans. Ind. Electron. 64 (10) (2017) 8193–8205.
[28] J.F. Lozano, N. Seoane, E. Comesaña, F. Almonacid, E.F. Fernández, A. García-Loureiro, Laser power converter architectures based on 3C-SiC with efficiencies >80 %, Solar RRL 6 (8) (2022) 2101077.
[29] J.F. Lozano, N. Seoane, E. Comesaña, F.M. Almonacid, E.F. Fernández, A. García-Loureiro, A new path towards ultra-high efficient laser power converters: silicon carbide-based multijunction devices, Results Eng. 21 (2024) 101987.
[30] F. Roccaforte, M. Leszczynski, Introduction to Gallium Nitride Properties and Applications, Wiley, 2020, pp. 1–39. https://doi.org/10.1002/9783527825264.ch1
[31] A. Udabe, I. Baraia-Etxaburu, D.G. Diez, Gallium nitride power devices: a state of the art review, IEEE Access 11 (2023) 48628–48650.
[32] I.C. Kizilyalli, A.P. Edwards, O. Aktas, T. Prunty, D. Bour, Vertical power p-n diodes based on bulk GaN, IEEE Trans. Electron Devices 62 (2) (2015) 414–422.
[33] V. Bermudez, D. Koleske, A. Wickenden, The dependence of the structure and electronic properties of wurtzite GaN surfaces on the method of preparation, Appl. Surf. Sci. 126 (1–2) (1998) 69–82.
[34] Z. Hu, K. Nomoto, B. Song, M. Zhu, M. Qi, M. Pan, X. Gao, V. Protasenko, D. Jena, H.G. Xing, Near unity ideality factor and Shockley-Read-Hall lifetime in GaN-on-GaN p-n diodes with avalanche breakdown, Appl. Phys. Lett. 107 (24) (2015).
[35] S. Logothetidis, J. Petalas, M. Cardona, T.D. Moustakas, Optical properties and temperature dependence of the interband transitions of cubic and hexagonal GaN, Phys. Rev. B 50 (24) (1994) 18017–18029.
[36] A. Dmitriev, A. Oruzheinikov, The rate of radiative recombination in the nitride semiconductors and alloys, J. Appl. Phys. 86 (6) (1999) 3241–3246.
[37] Y. Aoki, M. Kuwabara, Y. Yamashita, Y. Takagi, A. Sugiyama, H. Yoshida, A 350-nm-band GaN/AlGaN multiple-quantum-well laser diode on bulk GaN, Appl. Phys. Lett. 107 (15) (2015) 151103.
[38] F. Wu, H. Sun, I.A. AJia, I.S. Roqan, D. Zhang, J. Dai, C. Chen, Z.C. Feng, X. Li, Significant internal quantum efficiency enhancement of GaN/AlGaN multiple quantum wells emitting at 350 nm via step quantum well structure design, J. Phys. D Appl. Phys. 50 (24) (2017) 245101.
[39] G.Y. Zhao, H. Ishikawa, H. Jiang, T. Egawa, T. Jimbo, M. Umeno, Optical absorption and photoluminescence studies of n-type GaN, Jpn. J. Appl. Phys. Part 2 Lett. 38 (9A) (1999) L993.
[40] G. Sabui, P.J. Parbrook, M. Arredondo-Arechavala, Z.J. Shen, Modeling and simulation of bulk gallium nitride power semiconductor devices, AIP Adv. 6 (5) (2016).
[41] S. Logothetidis, J. Petalas, M. Cardona, T.D. Moustakas, The optical properties and electronic transitions of cubi and hexagonal GaN films between 1.5 and 10 eV, Mater. Sci. Eng. B 29 (1–3) (1995) 65–69.
[42] T.T. Mnatsakanov, M.E. Levinshtein, L.I. Pomortseva, S.N. Yurkov, Carrier mobility model for simulation of sic-based electronic devices, Semicond. Sci. Technol. 17 (9) (2002) 974–977.
[43] N. Arora, J. Hauser, D. Roulston, Electron and hole mobilities in silicon as a function of concentration and temperature, IEEE Trans. Electron Devices 29 (2) (1982) 292–295.
[44] Y. Varshni, Temperature dependence of the energy gap in semiconductors, Physica 34 (1) (1967) 149–154.
[45] F. Olivier, A. Daami, C. Licitra, F. Templier, Shockley-read-hall and auger non-radiative recombination in GaN based leds: a size effect study, Appl. Phys. Lett. 111 (2) (2017).
[46] K.A. Bulashevich, S.Y. Karpov, Impact of surface recombination on efficiency of iii-nitride light-emitting diodes, Phys. Status Solidi - Rapid Res. Lett. 10 (6) (2016) 480–484.
[47] W.G. Scheibenzuber, U.T. Schwarz, L. Sulmoni, J. Dorsaz, J.F. Carlin, N. Grandjean, Recombination coefficients of GaN-based laser diodes, J. Appl. Phys. 109 (9) (2011).
[48] J.S. Im, A. Moritz, F. Steuber, V. Härle, F. Scholz, A. Hangleiter, Radiative carrier lifetime, momentum matrix element, and hole effective mass in GaN, Appl. Phys. Lett. 70 (5) (1997) 631–633.
[49] T. Shan, X. Qi, Design and optimization of GaAs photovoltaic converter for laser power beaming, Infrared Phys. Technol. 71 (2015) 144–150.
[50] Silvaco, Silvaco software (version 5.30.0.R), 2020, https://www.silvaco.com.
[51] M. Ochoa, E. Barrigón, L. Barrutia, I. García, I. Rey-Stolle, C. Algora, Limiting factors on the semiconductor structure of III–V multijunction solar cells for ultra-high concentration (1000–5000 suns), Prog. Photovolt. Res. Appl. 24 (10) (2016) 1332–1345.
[52] C. Honsberg, S. Bowden, Effect of temperature. https://www.pveducation.org/pvcdrom/solar-cell-operation/effect-of-temperature?expr=600 (pveducation.org).
[53] A. Maros, S. Gangam, Y. Fang, J. Smith, D. Vasileska, S. Goodnick, M.I. Bertoni, C.B. Honsberg, High temperature characterization of GaAs single junction solar cells, in: 2015 IEEE 42nd Photovoltaic Specialist Conference (PVSC), 2015, pp. 1–5, https://doi.org/10.1109/PVSC.2015. 7356338.
[54] J.F. Lozano, N. Seoane, E. Comesaña, F.M. Almonacid, E.F. Fernández, A. García-Loureiro, Accurate modelling of a GaAs-based laser power converter, in: 14th Spanish Conference on Electron Devices (CDE 2023), IEEE, 2023, pp. 29–30.